ELSEVIER

Earth and Planetary Science Letters 5666 (2000) 1–15

EPSL

www.elsevier.com/locate/epsl

Wavelet analysis of relative geomagnetic paleointensity at ODP Site 983

Yohan Guyodo [a,*], Philippe Gaillot [b,c,d], James E.T. Channell [a]

[a] *Department of Geological Sciences, 241, University of Florida, Williamson Hall, Gainesville, FL 32611, USA*
[b] *CNRS UMR 7516, Imagerie Tectonique, Université Louis Pasteur, Strasbourg, France*
[c] *CNRS UMR 5563, Pétrophysique et Tectonique, Université Paul Sabatier, Toulouse, France*
[d] *Laboratoire de Mesures en Forage, ISTEEM, Université de Montpellier, Montpellier, France*

Received 3 July 2000; received in revised form 12 October 2000; accepted 12 October 2000

Abstract

We performed a spectral analysis of a record of relative geomagnetic paleointensity obtained at ODP Site 983, covering the time interval 0–1.1 Ma. The results confirm the presence of significant power at frequencies corresponding to the earth orbital parameters (eccentricity, obliquity, precession). The construction of the evolutionary spectrum allowed us to establish the non-stationarity of the signal at those frequencies. The subsequent use of wavelet techniques made it possible to demarcate the time intervals over which orbital frequencies are present in the record. For those intervals, the paleointensity record shows some coherency with the isothermal remanent magnetization, normalizer of the natural remanent magnetization, and the ratio anhysteretic remanent magnetization/*k*. These results suggest that the orbital frequencies embedded in the paleointensity record are the expression of lithologic variations, and probably not a characteristic of the geodynamo itself. Extracting (filtering) these wavelet components from the Site 983 paleointensity record indicates, however, that this secondary overprint is of sufficiently low level that it has a minor effect on the overall character of the record.

Keywords: paleomagnetism; wavelet analysis; magnetic intensity; spectral analysis

1. Introduction

In the past 10 yr, more than 30 sedimentary records of relative paleointensity of variable resolutions and durations have been published (e.g. [1–15]). This fast growing database is believed to reflect the time evolution of the geomagnetic dipole field intensity, hence constraining the models aimed at describing the processes governing the geodynamo. Evidence for the reliability of sedimentary records of relative paleointensity is provided by the high degree of correlation between individual records from different regions of the world [15–18,32]. Additional proof comes from the covariance of these records with paleointensity proxies derived from cosmogenic radionuclides such as ^{10}Be and ^{36}Cl [19–21]. Since geomagnetic intensity may vary on a global scale, the use of relative paleointensity records as a correlative tool is of great interest. Relative paleointensity stratigraphy may offer a time resolution greater than

* Corresponding author. Tel.: +1-352-392-2231; E-mail: guyodo@ufl.edu

0012-821X/00/$ – see front matter
PII: S0012-821X(00)00313-7

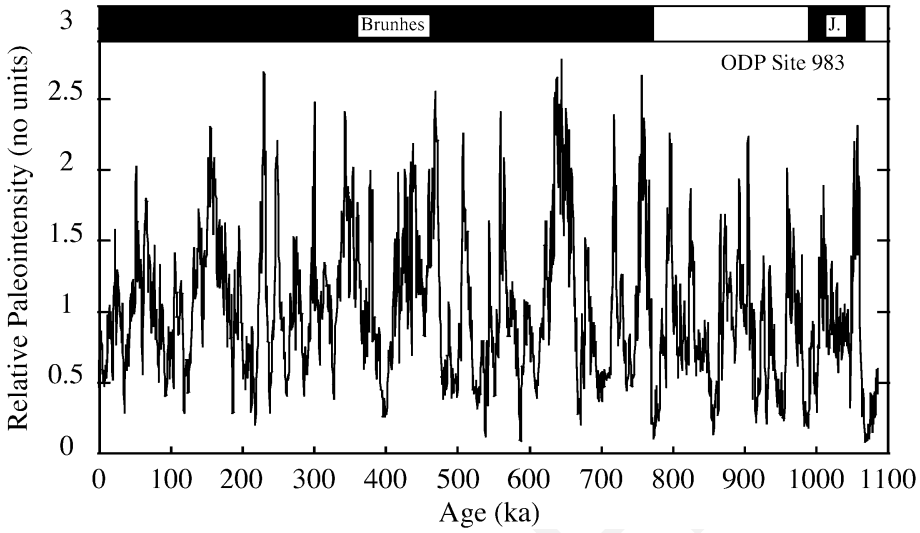

Fig. 1. Relative geomagnetic paleointensity record at ODP Site 983.

$\delta^{18}O$ techniques, which could be of crucial importance for correlation and dating of climate proxy records in sediments. Integration of these paleointensity records [15–17] into composite records has provided target curves (NAPIS-75, Sint-200, Sint-800) for the last 800 000 yr. Significant refinement of these curves will be achieved with additional high quality records, and the routine use of quantitative methods of investigation such as jackknife techniques, coherence function spectrum, and in some cases wavelet analysis.

The scope of our paper is to present the wavelet analysis of a recently published record of relative paleointensity form Ocean Drilling Program (ODP) Leg 162 Site 983 [1–3]. Site 983 (60.4°N, 23.64°W) is of particular interest because it provided a high latitude, high resolution paleomagnetic record (average sedimentation rate of 12.3 cm/kyr), characterized by a high density of age calibration points. The magnetic properties were measured on U-channel samples [22], using the 2-G enterprises pass-through magnetometers located at Gif-sur-Yvette (France) and at the University of Florida [23,24]. The natural remanent magnetization (NRM), the anhysteretic remanent magnetization (ARM), and the isothermal remanent magnetization (IRM) were progressively alternating field-demagnetized, and measured at each demagnetization step [1–3]. The magnetic susceptibility (k), the ARM, and the IRM were used to normalize the NRM for variations in concentration of magnetic grains and construct paleointensity proxies. Comparison of the three estimates for several demagnetization steps pointed to the ratio NRM/IRM as the best paleointensity proxy at this site [1–3].

An initial spectral investigation of the ODP Site 983 paleointensity record was performed for the interval 0–725 ka [2]. The power spectrum revealed the existence of significant power at the earth orbital eccentricity (0.01 kyr^{-1}, 100 kyr) and obliquity (0.0244 kyr^{-1}, 41 kyr) frequencies. A similar analysis was performed on the bulk magnetic parameters, and showed that the cycles at 100 kyr were present in all the records. The paleointensity signal at 100 kyr was therefore attributed to a lithologic overprint. In contrast, the 41 kyr cycles were not observed in the bulk magnetic parameters, and it was concluded that the obliquity cycles observed in the paleointensity record may be geomagnetic in origin, and that the geodynamo may be influenced by the orbital obliquity. Another spectral analysis on the interval 700–1100 ka yielded similar results [3]. The signal to noise ratio in the bulk magnetic parameters is however relatively low for these frequencies so that small intervals with significant power at orbital frequencies may have been missed by the

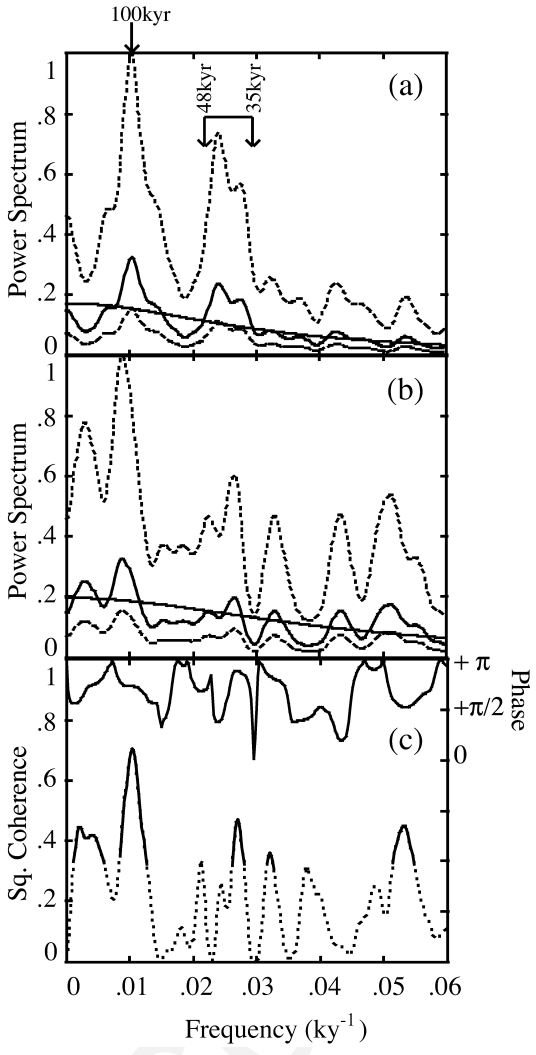

Fig. 2. Power spectra of (a) the relative paleointensity record and (b) he IRM record at ODP Site 983. The sloping lines represent the best fit estimates for the background (red noise) spectra. The dashed lines correspond to the confidence limits at the 95% confidence level. (c) Coherence function (square coherence and phase) between the paleointensity record and the IRM. The dashed line corresponds to signals below the 95% confidence level.

initial Fourier analysis. Given the high resolution and superior age control in this record, it provides a unique opportunity to try spectral methods of greater resolution. The present study concerns the entire paleomagnetic record, covering the last 1100 kyr (Fig. 1). Over this interval, we applied wavelet analysis techniques in search of potential non-stationarities, and to investigate the possibility of previously undetected coherency between the paleointensity signal and the bulk magnetic parameters.

2. Spectral analysis

2.1. Global power spectrum

Fig. 2 represents the global power spectrum calculated for the paleointensity and the IRM (normalizer) records, along with the associated coherence function (squared coherence and phase). The spectrum was obtained using the Blackman–Tukey method and a Bartlett window [25]. The power spectrum calculated for the 0–1100 ka paleointensity record reveals two maxima associated with frequencies close to those of the earth orbital parameters (Fig. 2). A first significant peak is found at 0.01 kyr^{-1} (100 kyr), and a second broader peak is found between 0.021 kyr^{-1} (48 kyr) and 0.029 kyr^{-1} (35 kyr). In contrast to the first analysis performed over the interval 0–725 ka [2], the peak at 0.0244 kyr^{-1} (41 kyr) is a double peak (first maximum at 0.0240 kyr^{-1} and second at 0.0273 kyr^{-1}). This could be the result of some inaccuracies in dating, or the expression of the various dynamics of the system (e.g. different levels of climate overprint added to a stochastic geomagnetic signal, or real evolution of the time scales inherent to the geodynamo). As

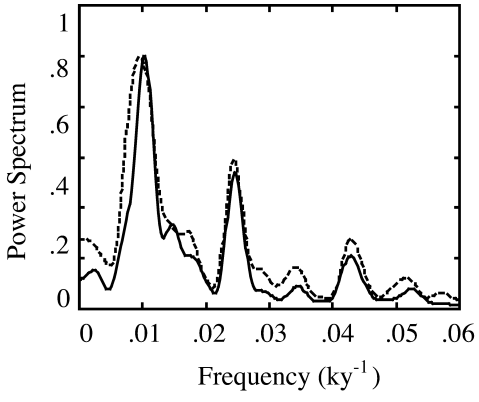

Fig. 3. Power spectra of the benthic (solid line) and planktic (dashed line) $\delta^{18}O$ records at Site 983.

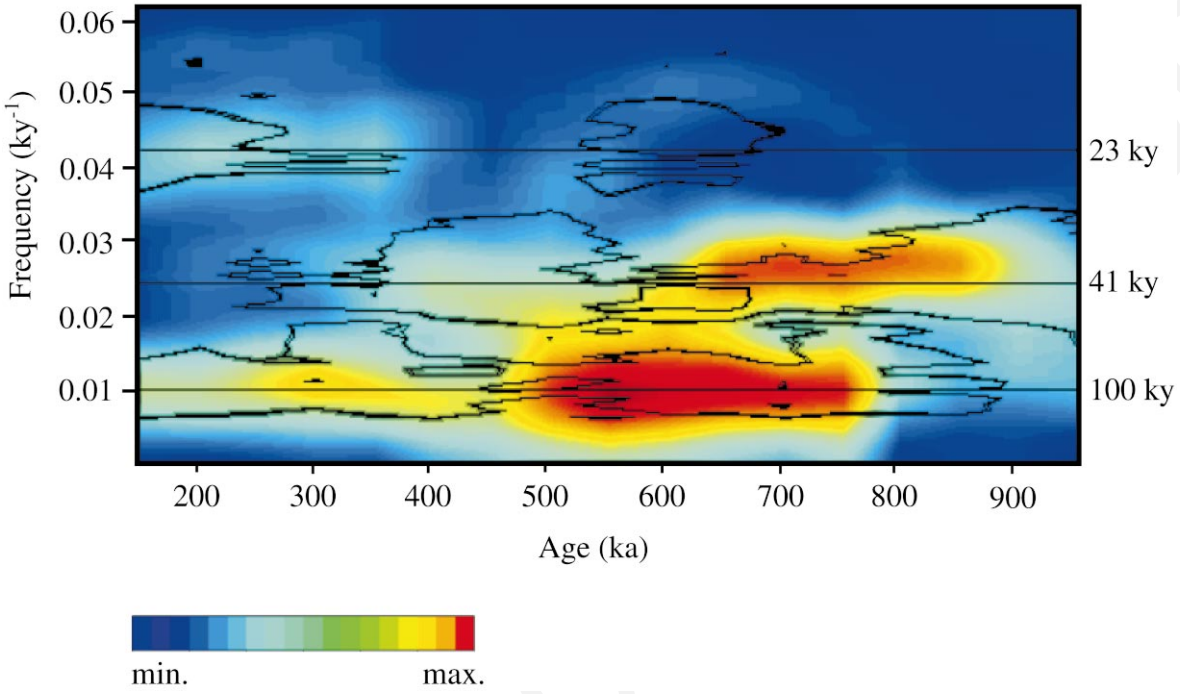

Fig. 4. Evolutionary power spectrum of the paleointensity record at Site 983. The spectrum was obtained using a sliding window of 300 kyr width and steps of 50 kyr. The contour lines correspond to the best fit estimate of the background spectrum.

a check, we applied the same spectral analysis to the benthic and planktic $\delta^{18}O$ records which were used to construct the age model (Fig. 3). They yielded very clear power spectra, with a sharp peak at 41 kyr showing that the double peak observed in the paleointensity power spectrum is not due to dating inaccuracies. In addition, some coherency can be observed between the IRM and the paleointensity for periods close to the eccentricity and the obliquity. As already mentioned, no such coherency was observed in the previous spectral analyses of the data [2,3], which might be due to the fact that we performed our analysis over a much longer interval, therefore slightly increasing the signal to noise ratio. However, the IRM spectrum is still very close to the one of red noise (Fig. 2), suggesting some caution in the interpretation of this apparent coherence. A better understanding of the origin of these signals may arise from the reconstruction of the time evolution of the power spectrum.

2.2. Evolutionary power spectrum

One way of assessing the time evolution of a time series power spectrum is to compute the evolutionary power spectrum of that series, which can be represented as a color diagram displaying ages on the horizontal axis, frequencies on the vertical axis, and indexed colors for the power spectrum. We constructed the evolutionary spectrum of the ODP Site 983 paleointensity record by calculating the power spectrum of the time series within a sliding window of 300 kyr width and a translation step of 50 kyr, using the same spectral method as for the global spectrum (Fig. 4). The results show that the spectral content of the paleointensity record is time dependent. The last $\sim$800 kyr is the only time interval when the signal corresponding to the eccentricity (100 kyr, 0.01 kyr^{-1}) is present. The bandwidth associated with the obliquity (41 kyr, 0.0244 kyr^{-1}) is observed only between $\sim$400 ka and $\sim$900 ka, and displays a frequency shift around $\sim$600 ka. This observation accounts for the two peaks ob-

served in the global power spectrum, which may be interpreted as a result of the time dependency of the power spectrum. However, it does not tell us about the origin of the signal, nor if these two peaks are the expression of the obliquity only, or a combination of several signals including the obliquity. The signal in this spectral band drops below the background spectrum (as defined by the red noise spectrum associated with this record) around ~600 ka, over an interval of ~100 kyr. This indicates that the spectral content of the paleointensity record varies over time scales shorter than the window used to calculate the power spectra (i.e. 300 kyr). As a consequence, although the evolutionary spectrum represents an improvement relative to the global approach, it is inappropriate for resolving the small time scales present in this record. A better resolution of the periodicity around 41 kyr could be obtained by reducing the size of the sliding window. However, it would generate aliasing of the lower frequencies and reduce the quality of the output at that scale. In order to solve this problem, we must use a method providing spectral information that is scale independent. The wavelet transform is a good candidate for such a task [26–28].

3. Wavelet analysis

3.1. Description of the method

Wavelet analysis provides an automatic localization of specific behaviors such as cyclic patterns or discontinuities, both in time and frequency (e.g. [26,27]). In contrast to the Fourier transform which is computed using a single time window of constant width, the wavelet transform is a multi-scale method that uses narrow windows at high frequencies and wide windows at low frequencies [28]. Therefore, wavelet analysis contrasts strongly with the classical Fourier transform and windowed spectral analysis, which do not detect temporal discontinuities, are not able to distinguish between continuous low-amplitude and non-stationary high-amplitude signals, and do not provide information on the temporal persistence of periodicities. The continuous wavelet

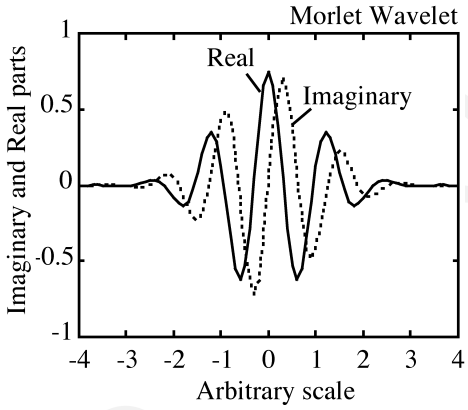

Fig. 5. The Morlet wavelet used to compute the wavelet transform. The solid line corresponds to the real part of the wavelet function, and the dashed line to its imaginary part.

transform of a time series $f(t)$ is defined as:

$$W_{\Psi}(a,b) = \frac{1}{\sqrt{a}} \int_T f(t)\, \Psi\left(\frac{1-b}{a}\right) \mathrm{d}t \qquad (1)$$

where Ψ is a base wavelet characterized by a length much shorter than the time series $f(t)$, and a, b, and T correspond to the dilatation scales, translation steps, and time length of the wavelet transform, respectively. The wavelet $\Psi(t)$ must be a function with compact support and zero mean. The second property (admissibility condition) ensures that $\Psi(t)$ has a wiggle (i.e. is wave like), and the first ensures that it is not a sustaining wave. In the present paper, we use the Morlet wavelet [26,29] because its shape is similar to a periodic sinusoidal function, suitable for investigating periodicities (Fig. 5). The Morlet wavelet $\Psi(t) = \pi^{-1/4} e^{i\omega_0 t} e^{-t^2/2}$ (in our case $\omega_0 = 5$) is a complex valued function enabling extraction of information on both the amplitude and phase of the process being analyzed. The normalizing constant $1/\sqrt{a}$ is chosen so that $\Psi_a(t)$ has the same energy for all scales. The scale parameter (or dilatation factor), a, determines the characteristic frequencies at which the wavelet transform is computed. In our case, the dilatation scales were chosen so that the equivalent Fourier periods are given by $2^{k\delta k} t_0$, where t_0 is the sampling rate of the time series (Fourier period = 1.224 a) (see [27]). The parameter $k\delta k$ is chosen so that it is

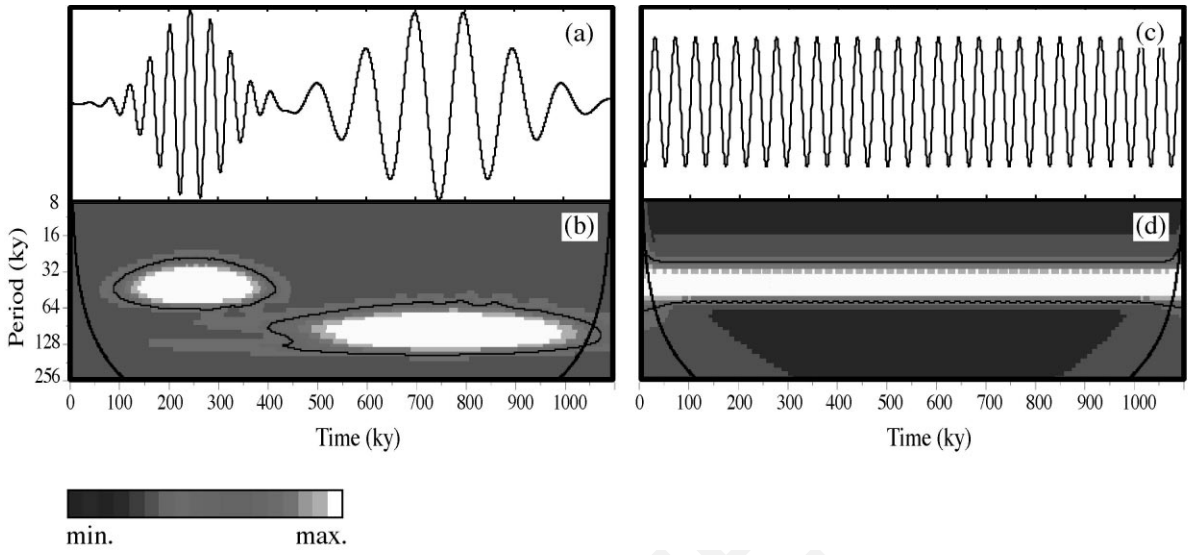

Fig. 6. Examples of wavelet spectra obtained for synthetic time series, with the ages on the horizontal axis and the equivalent Fourier periods on the vertical axis; the modulus of the wavelet transform being represented by indexed colors. This type of diagram is therefore comparable in its representation to an evolutionary power spectrum. The first series contains (a) two periodic signals (41 kyr, 100 kyr) over different intervals, which are identifiable as white patches on the wavelet spectrum (b). The second series (c) has a single frequency, which yielded a clear wavelet spectrum (d). The contour lines represent the confidence level at 95%. The thick black lines on the left and right edges of the spectra indicate the regions of the diagram where the edge effects become important.

possible to cover the Fourier domain of interest (here the one containing periods of 23 kyr, 41 kyr, and 100 kyr) with an appropriate resolution [27]. A reading of the wavelet power spectrum can be obtained by constructing a color diagram with the ages on the horizontal axis and the scales (or the equivalent Fourier periods) on the vertical axis; the modulus of the wavelet transform being represented by colored patches [27]. This type of diagram is therefore comparable to an evolutionary power spectrum, and can be revealing about the structure of a particular process. The main difference between the wavelet and the Fourier decompositions is in the support of the respective basis functions. The wavelet transform coefficients are influenced by local events, while the Fourier coefficients are influenced by the function in its entire domain. This makes the wavelet spectrum a better measure of the variance attributed to localized events (see [28]). Fig. 6 represents the wavelet power spectra of two synthetic time series $x_1(t)$ and $x_2(t)$. The first series $x_1(t)$ is a modulated function containing periodic signals at 41 kyr and 100 kyr. The second function $x_2(t)$ was constructed from a sinusoidal function of period 41 kyr in quadrature with $x_1(t)$. The wavelet power spectra in Fig. 6 show the modulations characterizing $x_1(t)$, as well as the time intervals over which the 41 kyr and the 100 kyr signals are actually present.

In order to facilitate the interpretation of this type of diagram, one can define a level above which a maximum in the wavelet spectrum or in the cross-wavelet power is statistically significant. It has been shown that each point in the wavelet power spectrum is statistically distributed as a χ^2 distribution with two degrees of freedom about the background spectrum [27]. The confidence level at each scale is therefore the product of the background spectrum and the desired significance level (for instance 95% confidence) from the χ^2 distribution. Here, the background spectrum is determined by calculating the time-average of the wavelet spectrum [27]. Similarly, the confidence levels of the cross-wavelet spectrum can

be derived from the square root of the product of two χ^2 distributions [27,30].

In addition to the wavelet power spectrum, it is possible to construct the cross-wavelet spectrum $W^{xy}{}_{\Psi} = W^{x}{}_{\Psi} W^{y*}{}_{\Psi}$ of two time series $x(t)$ and $y(t)$ from their respective wavelet transforms $W^{x}{}_{\Psi}$ and $W^{y}{}_{\Psi}$ ($W^{y*}{}_{\Psi}$ is the complex conjugate of $W^{y}{}_{\Psi}$). Subsequently, cross-wavelet power (modulus) and phase can be extracted. Local maxima in power provide information about the scales at which coherent events have a significant contribution. In Fig. 7 we present the cross-wavelet power and phase of the synthetic series $x_1(t)$ and $x_2(t)$ from Fig. 6. The diagrams show that the covariance between the two series is limited to the first half of the records (i.e. where the 41 kyr period exists in both series). In addition, the cross-wavelet phase gives the phase relationship between the two series (here equal to π/2), which

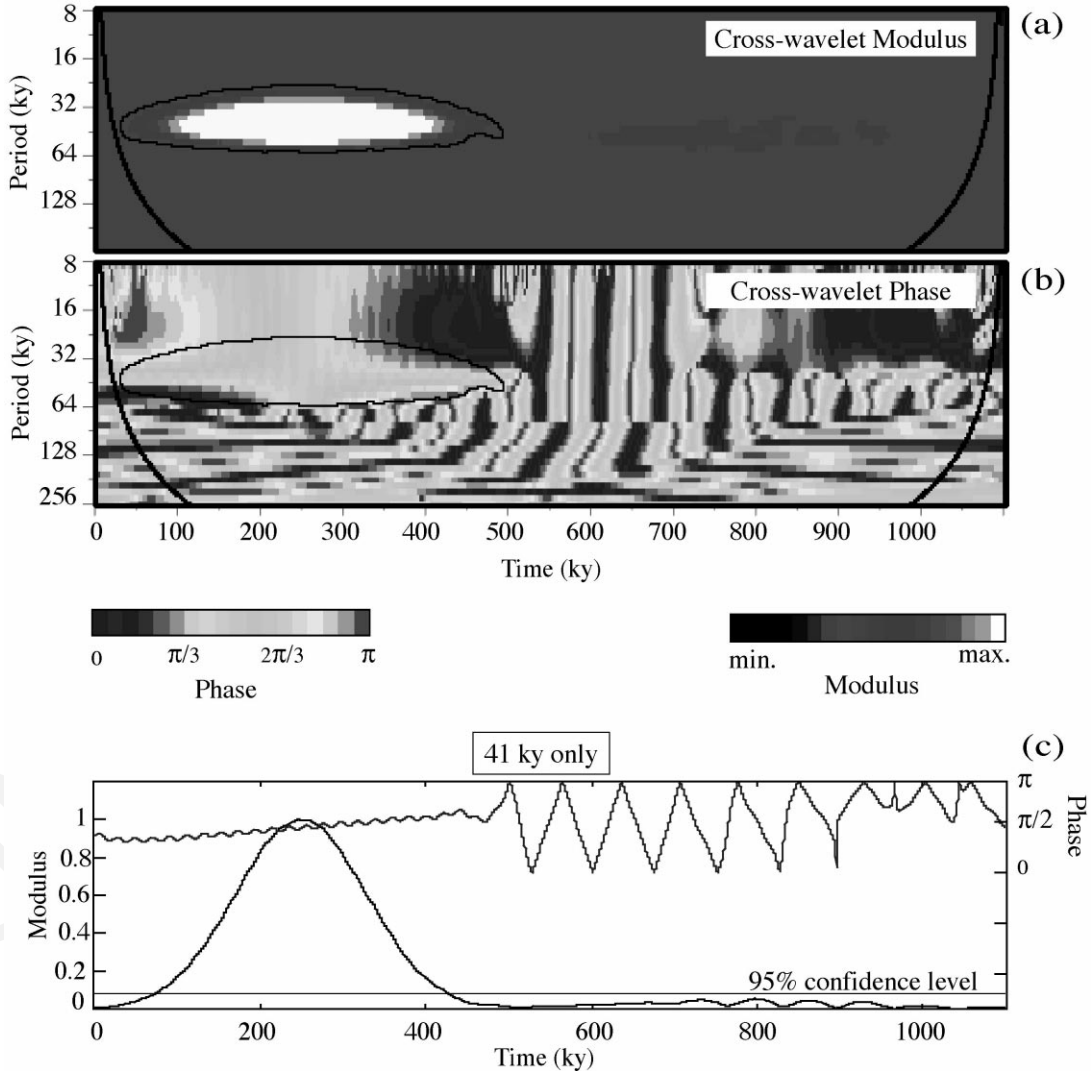

Fig. 7. Cross-wavelet spectrum (a) and phase (b) for the same two time series as in Fig. 6. The two series are coherent only over the first half of the record, over which they display a phase lag of π/2. (c) Cross-wavelet spectrum and phase for the 41 kyr Fourier period only.

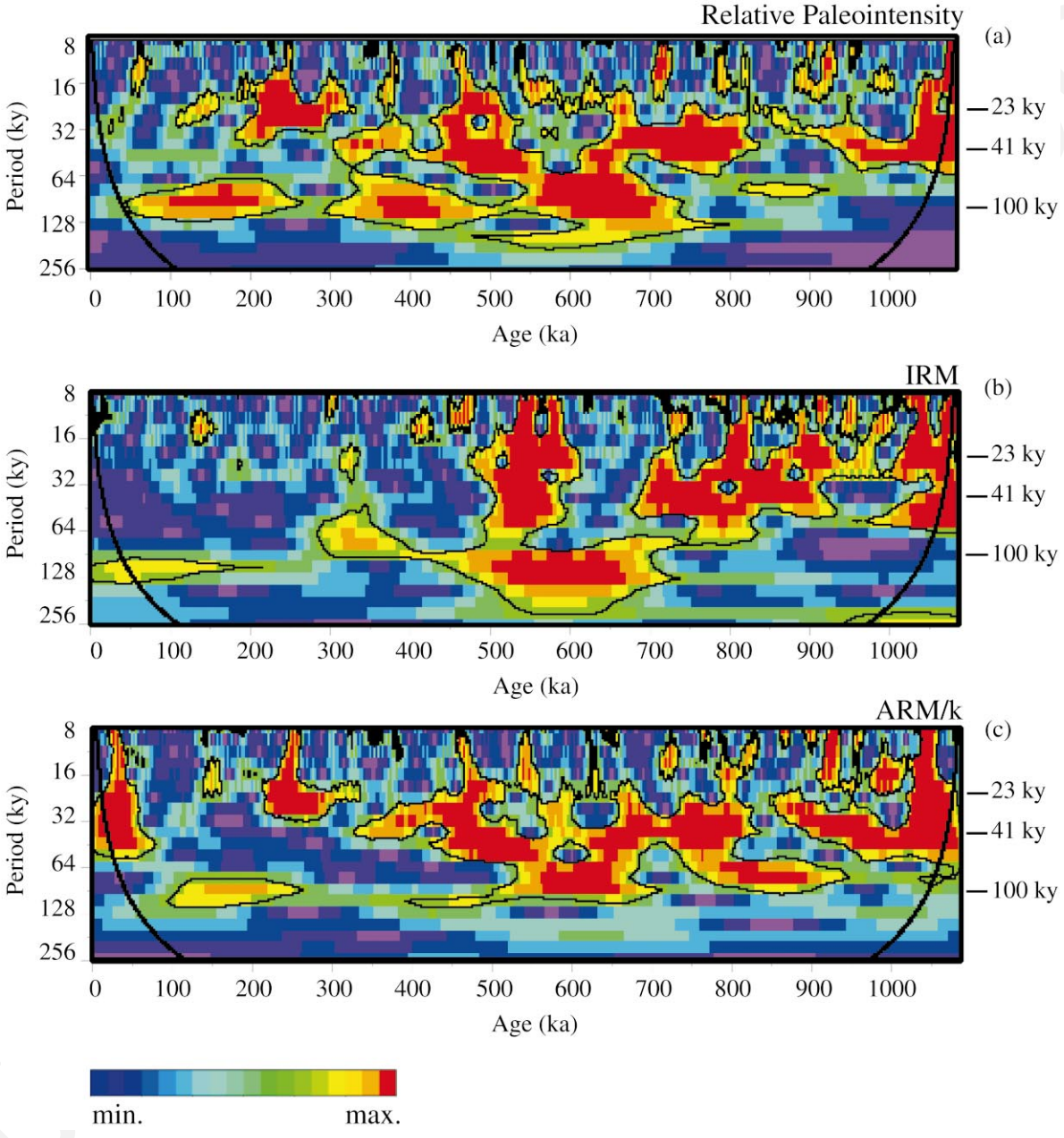

Fig. 8. (a) Wavelet spectrum of the paleointensity record at Site 983, showing the time intervals where significant power exists at frequencies corresponding to the earth orbital parameters. (b) Wavelet spectrum of IRM. (c) Wavelet spectrum of the ratio ARM/*k* (anhysteretic remanence divided by susceptibility).

is stable only over the interval containing the 41 kyr signal.

If one wants to focus on a specific scale (or the equivalent Fourier period), the cross-wavelet spectrum and phase can be represented for this particular scale only (Fig. 7c). This corresponds to a reading of the information provided by Fig. 7a,b along a horizontal line placed at 41 kyr.

3.2. Wavelet power spectrum of ODP Site 983 paleointensity record

We computed the wavelet transform of the relative paleointensity record at ODP Site 983. The wavelet power spectrum, modulus of the wavelet transform, is shown on Fig. 8a. Essentially, the features initially observed in the evolutionary power spectrum are depicted with more detail. The signal for the 100 kyr period (possibly the eccentricity signal) is restricted to the last ~750 kyr and shows some modulations, with three maxima centered at ~150 ka, ~400 ka, and ~650 ka. The signal at 41 kyr (obliquity) is observed over relatively short periods of time. Three main intervals can be distinguished: 400–550 ka, 650–825 ka, and 950–1100 ka. Furthermore, the apparent shift in frequencies observed in the evolutionary power spectrum does not appear on the wavelet spectrum. In contrast, it reveals the existence of a complex structure over the interval 400–550 ka, characterized by scales with equivalent Fourier periods ranging from 10 to 70 kyr. Therefore, only a small fraction of the intensity seems to be carried by the 41 kyr period signal over this interval, which accounts also for the shift observed in the evolutionary power spectrum. A few patches corresponding to the 23 kyr signal (precession) are also present in the wavelet power spectrum, essentially around ~250 ka, ~500 ka, and ~1050 ka. These intervals were barely detected by the evolutionary spectrum. In addition, several small-scale features of short duration are scattered though the wavelet spectrum. These features correspond to intervals in the paleointensity record characterized by large amplitude variations such as for instance the intervals 30–60 ka, or 100–160 ka (Figs. 1 and 8). These intervals of major change in relative paleointensity do not correspond to parts of the paleointensity records containing frequencies similar to the orbital obliquity.

In order to understand the origin (climatic overprint or orbital forcing in the geodynamo) of the periodic signals detected by the wavelet transform, we performed the same analysis on the IRM (Fig. 8b), which was used to normalize the NRM to yield the paleointensity proxy. As for the spectral method involving the calculation of coherence functions, a match between the wavelet spectrum of the paleointensity record and the one of the IRM indicates an incomplete normalization of the NRM. We also calculated the wavelet transform of the ratio ARM/k (Fig. 8c), which can be used as a proxy for relative changes in grain size of magnetite, the principal remanence carrier. Fig. 8b,c shows significant power in frequencies corresponding to the orbital parameters over time intervals similar to those of the paleointensity record (Fig. 8a). The existence of some intervals over which the IRM and the paleointensity records depict similar wavelet power spectra suggests that part of the lithologic component of the NRM was not completely removed by the normalization with IRM. The similarity between the paleointensity record and ARM/k (Fig. 8c) suggests that the NRM does not depend on the magnetic field and the magnetic concentration alone, but also on the magnetic grain size. This would explain why the IRM, influenced by the concentration of a particular grain size fraction, and not as sensitive to grain size as ARM/k, would not be able to fully normalize the NRM at orbital frequencies. A quantitative assessment of this covariance can be obtained by calculating the cross-wavelet spectrum between the paleointensity record and the magnetic parameters, following the same philosophy as when computing coherence function spectra from the global spectral analysis.

3.3. Cross-wavelet spectra

We calculated the cross-wavelet spectrum of the relative paleointensity record versus the IRM and the ratio ARM/k, and subsequently extracted cross-wavelet powers and phases. Instead of plotting these results in the form of contoured diagrams we have selected only the relevant scales for clarity (i.e. 23 kyr, 41 kyr, and 100 kyr). The results show significant covariance between the relative paleointensity record and both the IRM and the ratio ARM/k in specific intervals of the time series (Fig. 9). For each frequency, this covariance is observed over the same time intervals as those showing significant power in the paleo-

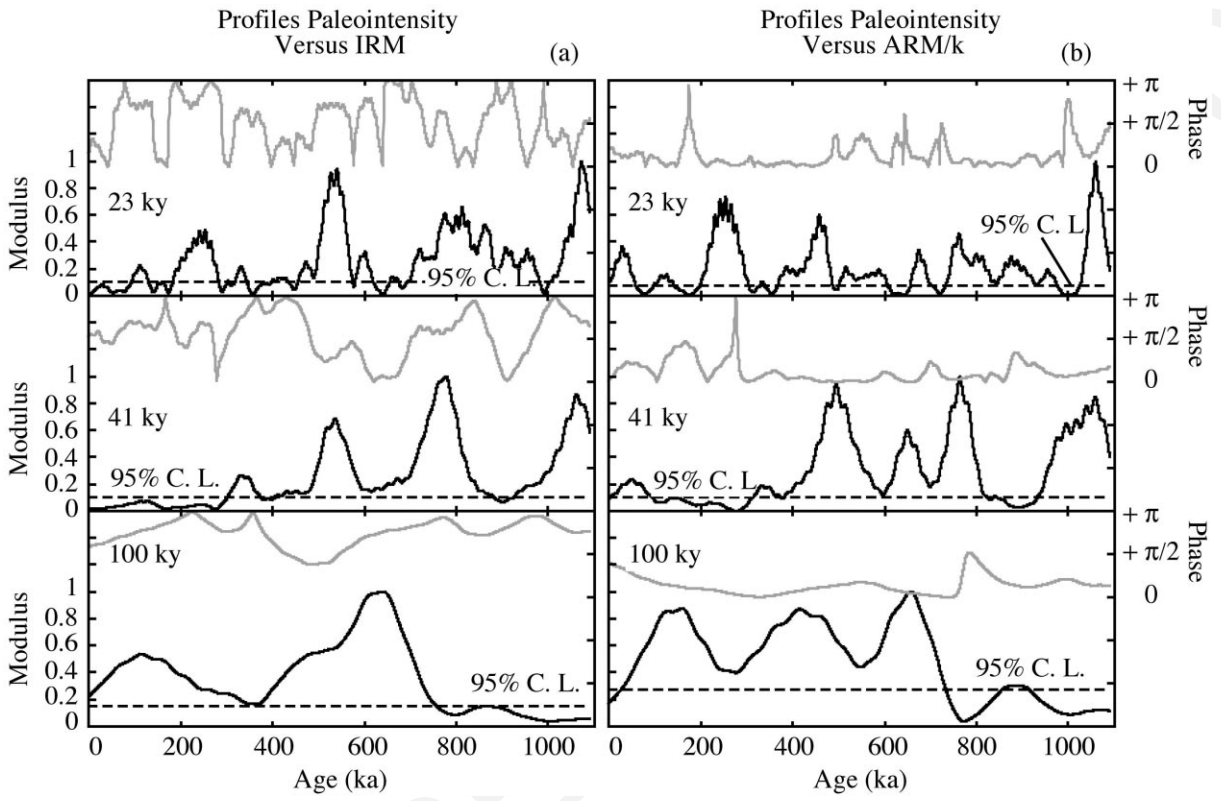

Fig. 9. Cross-wavelet spectra (black lines = power and gray lines = phase) of (a) the paleointensity record versus the IRM and (b) the paleointensity record versus the ratio ARM/k. We selected the scales corresponding to the earth orbital parameters.

intensity. When a high correlation is observed, the paleointensity signal tends to have inverse phase with respect to IRM, while it is in phase with ARM/k. This may be the consequence of a secondary dependency of the NRM on the magnetic grain size. In order to test the plausibility of this hypothesis, we constructed a simple synthetic model in which the NRM was simulated by a time series:

$$S1(t) = (0.8\ S2(t) + 0.2\ S3(t))S4(t)$$

where S2(t) represents a model of magnetic concentration (depicted by the IRM) and S3(t) a model of magnetic grain size (depicted by the ratio ARM/k), and S4(t) the geomagnetic field. The two other series, S2(t) and S3(t) were constructed from red noise spectra with the addition of two sinusoidal signals of periods 100 kyr and 41 kyr. The synthetic paleointensity record was then calculated by normalizing S1(t) with S2(t) (Fig. 10). We also calculated the coherence functions between the paleointensity model S5(t) and the parameters S2(t) and S3(t). Fig. 10 indicates that a slight grain size dependency of the NRM would induce significant covariance of the relative paleointensity with IRM, as well as with the ratio ARM/k. In addition, the paleointensity would be in phase with the ratio ARM/k and in opposition of phase with the IRM. The coherence functions were calculated over the entire interval, since the periodic signals built into the series were steady, and provided results showing strong correlations. There is no doubt that increasing the complexity of the model, by involving modulation of the periodic signals, different noise spectra, and abrupt changes in lithology and sedimentation rates would provide more realistic results such as those presented in Fig. 9. In any case, this very simple model provides a good, and rather

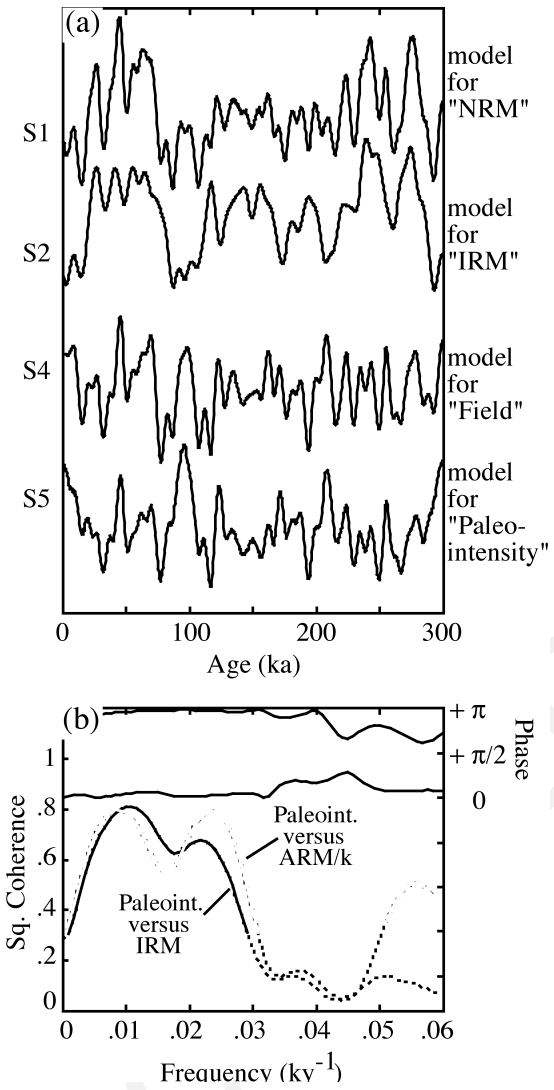

Fig. 10. Synthetic model aimed at explaining the observed coherency between the paleointensity record and the magnetic properties. (a) Models for S1(t) (NRM), S2(t) (IRM), S4(t) (geomagnetic field), and S5(t) = S1(t)/S2(t) (relative paleointensity). Notice that the paleointensity variations are very similar to the model for geomagnetic variations. (b) Coherence transforms of model paleointensity versus model IRM (in black) and versus model ARM/k.

simple explanation of the cross-wavelet spectra obtained for the Site 983 relative paleointensity record. One positive outcome of this model is that an incomplete normalization of the NRM over specific time intervals would not diminish the overall character of the paleointensity record. Indeed, the series S4(t) (field model) and S5(t) (paleointensity model) display very similar features, and are correlated with a high correlation coefficient of 0.75 (Fig. 10). This conclusion comes in support of other studies [14,16–18] showing that paleointensity records with different lithologies and sedimentation histories, including the present dataset, can be correlated over high distances with a large degree of confidence.

4. Conclusion

The present study confirms prior analyses showing the existence of periodic signals embedded into the paleointensity record at ODP Site 983 [1–3]. These signals correspond to the earth orbital eccentricity (100 kyr), obliquity (41 kyr), and precession (23 kyr). Calculation of the evolutionary power spectrum for the paleointensity record over the interval 0–1.1 Ma established the non-stationarity of these periodic signals, which display amplitude variations and are restricted to specific time intervals. The duration of these amplitude modulations appears to be smaller than the sliding window used to construct the evolutionary spectrum (300 kyr), calling for the use of more suitable spectral methods.

The use of wavelet analysis allowed us to define with greater precision the intervals over which the orbital frequencies are present in the record. The signal for the 100 kyr period (eccentricity) is restricted to the interval 0–750 ka and shows some modulations, with three maxima centered at ~150 ka, ~400 ka, and ~650 ka. The signal at 41 kyr (obliquity) is observed over relatively short periods of time. Three main intervals can be distinguished: 400–550 ka, 650–825 ka, and 950–1100 ka. The apparent absence of the 100 kyr period prior to ~750 ka, in the so-called 41 kyr world, may reflect the diminished influence of the eccentricity in climate proxy records. Other significant scales of variability were also recognized in the paleointensity record, resulting from the high complexity of the field which seems to be essentially non-stationary (see [31]). For the orbital frequencies, the paleointensity record shows

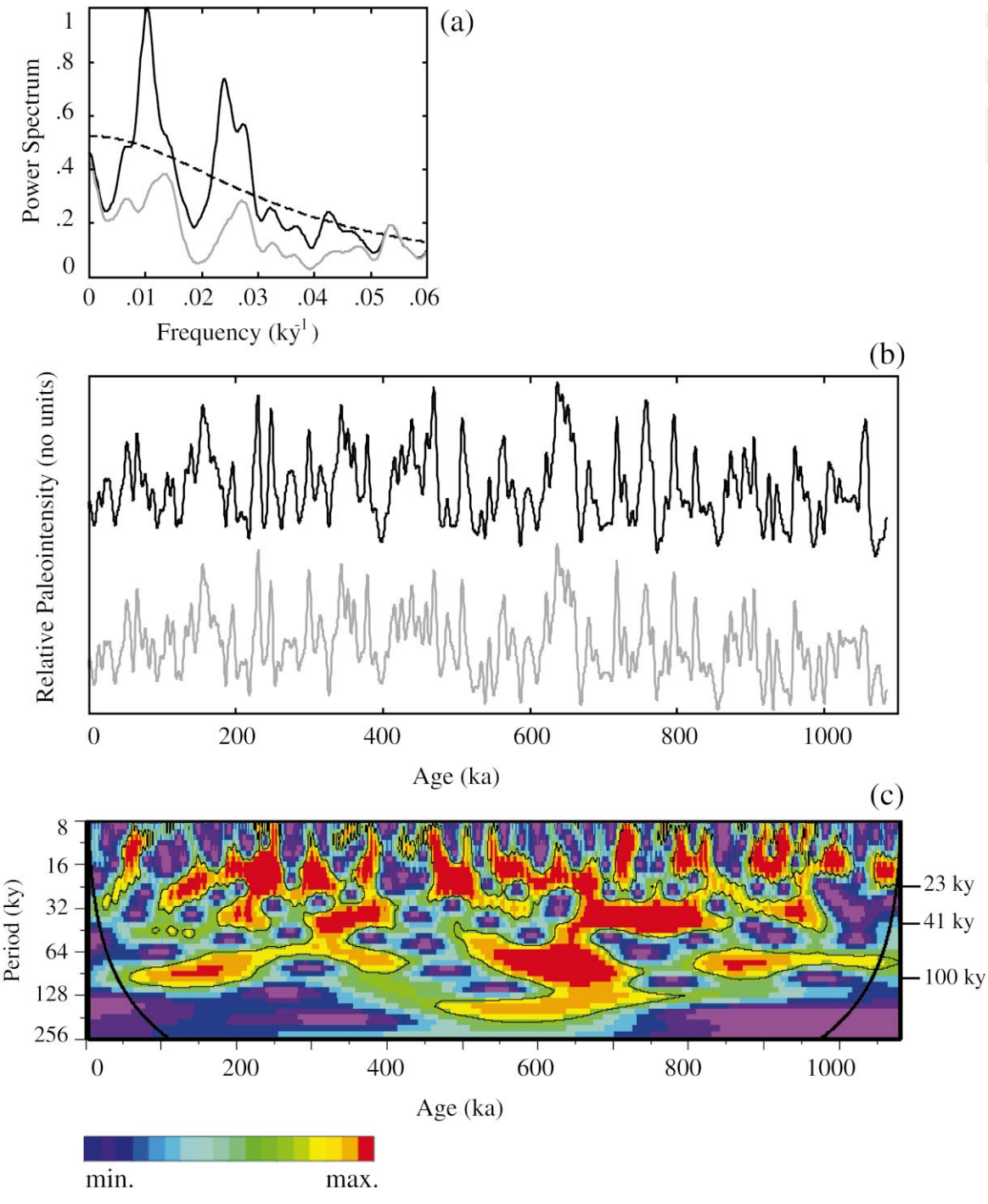
(a)
Power Spectrum
1
.8
.6
.4
.2
0
0
.01
.02
.03
.04
.05
.06
Frequency (ky^{-1})
(b)
Relative Paleointensity (no units)
0
200
400
600
800
1000
Age (ka)
(c)
Period (ky)
8
16
32
64
128
256
23 ky
41 ky
100 ky
0
200
400
600
800
1000
Age (ka)
min.
max.

Fig. 11. Filtering of the paleointensity record for the Fourier periods 23 kyr, 41 kyr, and 100 kyr. (a) The power spectrum of the original paleointensity record (in black) compared to that for the filtered paleointensity record (in gray) which is close to its background spectrum. (b) Comparison of the filtered (in gray) and the original (in black) paleointensity records. The filtered record was obtained by substraction of the wavelet components at 23 kyr, 41 kyr, and 100 kyr from the initial paleointensity record. In order to facilitate the comparison, the records were slightly smoothed using a singular spectrum analysis with three principal components. (c) Wavelet spectrum of the filtered paleointensity record, to be compared to the wavelet spectrum in Fig. 8a. ←

significant and stable covariance with the IRM and ARM/k over specific intervals of the record. This did not appear in previous spectral investigations of the paleointensity record [2,3] performed using standard spectral methods. Our study suggests that it is probably due to the limitations imposed by the global Fourier analysis, which is not always able to detect low-amplitude, locally distributed signals. Our wavelet analysis suggests the presence of a secondary lithologic overprint in the paleointensity record due to an incomplete normalization of the NRM. The results seem to be explained by simple models involving a slight magnetic grain size dependency of the NRM. The model shows also that the lithologic overprint does not drastically modify the paleointensity record, which remains very similar to the actual field model (Fig. 10).

Quantification of the amount of climatic overprint in the paleointensity record is not an easy task, nor is the normalization of this secondary component. In an attempt to estimate this overprint, we removed the orbital signals from the paleointensity record. As a first step, we extracted the wavelet components at (23 ± 5) kyr, (41 ± 5) kyr, and (100 ± 5) kyr. Then, we weighted the wavelet components with the cross-wavelet profiles of paleointensity versus ARM/k obtained for those frequencies, in order to restrict the filtering to the time intervals where a covariance between the two records exists. Evidently, the signal extracted contains information on both the overprint and the geomagnetic field. Indeed, the true geomagnetic signal contains variability at these time scales, as would any stochastic signal, which means that its power spectrum overlaps the one of ARM/k. The output signals were then substracted from the initial paleointensity variations. Fig. 11a shows the power spectrum of the resulting filtered signal, which does not seem to have any dominant Fourier period, compared with the global power spectrum of the original paleointensity record. The filtered paleointensity record does not seem to differ considerably from the initial record (Fig. 11b), with an overall difference of about $\sim 7\%$. The main changes reside in a reduction of some of the large amplitude variations present in the initial paleointensity record (Fig. 11b). The wavelet transform of the filtered paleointensity record (Fig. 11c) shows patches that are more uniformly distributed than for the initial paleointensity record (Fig. 8a). In particular, the regions of the spectrum corresponding to higher frequencies appear more clearly. This indicates the lesser dominance of specific oscillations, and that the filtered signal can be compared to a stochastic process. However, the extracted wavelet components are likely to contain some true geomagnetic signal over some intervals, or may have ignored some of the lithologic overprint (due to the restricted bandwidth of the filtering). An actual correction of the paleointensity signal would require quantification of the dual dependency of the NRM on the IRM and ARM/k, which is probably not constant throughout the time interval investigated. The paleointensity record at Site 983 has been shown to be correlatable at high resolution to other paleointensity records from the Labrador sea [18] and as far afield as the South Atlantic [32], suggesting that the lithologically controlled secondary overprint does not strongly affect the characteristic features of the paleointensity record, and probably does not impair its usefulness for stratigraphic correlation. However, for a quantitative assessment of the level of lithologic overprint in the record, multiple records, from various lithologies and different oceans need to be compared.

Acknowledgements

The authors thank Alain Mazaud and Carl Richter for their review of the manuscript. Discussions with Christopher Torrence resulted in improvement of our wavelet program. This research was partly supported by the US National Science Foundation (OCE 97-11424, EAR 98-04711).*[RV]*

References

[1] J.E.T. Channell, D.A. Hodell, B. Lehman, Relative geomagnetic paleointensity and $\delta^{18}O$ at ODP Site 983 (Gardar Drift, North Atlantic) since 350 ka, Earth Planet. Sci. Lett. 153 (1997) 103–118.

[2] J.E.T. Channell, D.A. Hodell, J. McManus, B. Lehman, Orbital modulation of geomagnetic paleointensity, Nature 394 (1998) 464–468.

[3] J.E.T. Channell, H.F. Kleiven, Geomagnetic palaeointensities and astrochronological ages for the Matuyama–Brunhes boundary and the boundaries of the Jaramillo Subchron: palaeomagnetic and oxygen isotope records from ODP Site 983, Phil. Trans. R. Soc. Lond. A 358 (2000) 1027–1047.

[4] E. Tric, J.-P. Valet, P. Tucholka, M. Paterne, L. Labeyrie, F. Guichard, L. Tauxe, M. Fontugne, Paleointensity of the geomagnetic field for the last 80 000 years, J. Geophys. Res. 97 (1992) 9337–9351.

[5] L. Meynadier, J.-P. Valet, R. Weeks, N.J. Shackleton, V.L. Hagee, Relative geomagnetic intensity of the field during the last 140 ka, Earth Planet. Sci. Lett. 114 (1992) 39–57.

[6] L. Meynadier, J.-P. Valet, F.C. Bassinot, N.J. Shackleton, Y. Guyodo, Asymmetrical saw-tooth pattern of the geomagnetic field intensity from equatorial sediments in the Pacific and Indian Oceans, Earth Planet. Sci. Lett. 126 (1994) 109–127.

[7] L. Tauxe, N.J. Shackleton, Relative paleointensity records from the Ontong–Java plateau, Geophys. J. Int. 117 (1994) 769–782.

[8] T. Yamazaki, N. Ioka, N. Eguchi, Relative paleointensity of the geomagnetic field during the Brunhes Chron, Earth Planet. Sci. Lett. 136 (1995) 525–540.

[9] T. Yamazaki, Relative paleointensity of the geomagnetic field during the Brunhes Chron recorded in the North Pacific deep-sea sediment cores: orbital influence?, Earth Planet. Sci. Lett. 169 (1999) 23–35.

[10] J.S. Stoner, J.E.T. Channell, C. Hillaire-Marcel, Late Pleistocene relative geomagnetic paleointensity from the deep Labrador sea: regional and global correlations, Earth Planet. Sci. Lett. 134 (1995) 237–252.

[11] D.A. Schneider, G.A. Mello, A high-resolution marine sedimentary record of geomagnetic intensity during the Brunhes Chron, Earth Planet. Sci. Lett. 144 (1996) 297–314.

[12] B. Lehman, C. Laj, C. Kissel, A. Mazaud, M. Paterne, L. Labeyrie, Relative changes of the geomagnetic field intensity during the last 280 kyear from piston cores in the Azores area, Phys. Earth Planet. Int. 93 (1996) 269–284.

[13] Y. Guyodo, C. Richter, J.-P. Valet, Paleointensity record from Pleistocene sediments (1.4–0 Ma) off the California Margin, J. Geophys. Res. 104 (B10) (1999) 22953–22964.

[14] J.-P. Valet, L. Meynadier, Geomagnetic field intensity and reversals during the past four million years, Nature 366 (1993) 234–238.

[15] C. Laj, C. Kissel, A. Mazaud, J.E.T. Channell, J. Beer, North Atlantic palaeointensity stack since 75 ka (NAPIS-75) and the duration of the Laschamp event, Phil. Trans. R. Soc. Lond. A 358 (2000) 1009–1025.

[16] Y. Guyodo, J.-P. Valet, Relative variations in geomagnetic intensity from sedimentary records: the past 200 thousand years, Earth Planet. Sci. Lett. 143 (1996) 23–36.

[17] Y. Guyodo, J.-P. Valet, Global changes in intensity of the Earth's magnetic field during the past 800 kyr, Nature 399 (1999) 249–252.

[18] J.S. Stoner, J.E.T. Channell, C. Hillaire-Marcel, A 200 kyr geomagnetic chronostratigraphy for the Labrador Sea: Indirect correlation of the sediment record to SPECMAP, Earth Planet. Sci. Lett. 159 (1998) 165–181.

[19] S. Baumgartner, J. Beer, J. Masarik, G. Wagner, L. Meynadier, H.-A. Synal, Geomagnetic modulation of the ^{36}Cl flux in the GRIP ice core, Greenland, Science 279 (1998) 1330–1332.

[20] M. Frank, B. Schwarz, S. Baumann, P.W. Kubik, M. Suter, A. Mangini, A 200 kyr record of cosmogenic radionuclide production rate and geomagnetic intensity field intensity from ^{10}Be in globally stacked deep-sea sediments, Earth Planet. Sci. Lett. 149 (1997) 121–129.

[21] M. Frank, Comparison of cosmogenic radionuclide production and geomagnetic field intensity over the last 200 000 years, Phil. Trans. R. Soc. Lond. A 358 (2000) 1089–1107.

[22] L. Tauxe, J.L. LaBrecque, R. Dodson, M. Fuller, U-channels – a new technique for paleomagnetic analysis of hydraulic piston cores, EOS Trans. AGU 64 (1983) 219.

[23] R. Weeks, C. Laj, L. Endignoux, M. Fuller, A. Roberts, R. Manganne, E. Blanchard, W. Goree, Improvements in long-core measurement techniques: applications in palaeomagnetism and palaeoceanography, Geophys. J. Int. 114 (1993) 651–662.

[24] E.A. Nagy, J.-P. Valet, New advances for paleomagnetic studies of sediment cores using U-channels, Geophys. Res. Lett. 20 (1993) 671–674.

[25] D. Paillard, L. Labeyrie, P. Yiou, Macintosh program performs time-series analysis, EOS Trans. AGU 77 (1996) 379.

[26] I. Daubechies, Ten Lectures on Wavelets, Soc. For Ind. And Appl. Math., Philadelphia, PA, 1992, 357 pp.

[27] C. Torrence, G. Compo, A practical guide to wavelet analysis, Bull. Am. Meteor. Soc. 79 (1998) 61–78.

[28] K.-M. Lau, H.-Y. Weng, Climate signal detection using wavelet transform: How to make a time series sing, Bull. Am. Meteor. Soc. 76 (1995) 2391–2402.
[29] J. Morlet, G. Arens, E. Fourgeau, D. Girard, Wave propagation and sampling theory, 2, Sampling theory and complex waves, Geophysics 47 (1982) 203–221.
[30] G.M. Jenkins, D.G. Watt, Spectral Analysis and its Applications, Holden-Day, 1968, 525 pp.
[31] T. Sato, H. Kikuchi, M. Nakashizuka, M. Okada, Quaternary geomagnetic field intensity: Constant periodicity or variable period?, Geophys. Res. Lett. 25 (1998) 2221–2224.
[32] J.E.T. Channell, J.S. Stoner, D.A. Hodell, C.D. Charles, Geomagnetic paleointensity for the last 100 kyr from the sub-antarctic South Atlantic: a tool for inter-hemispheric correlation, Earth Planet. Sci. Lett. 175 (2000) 145–160.